Multiscale Structure and Properties of Cast and Deformation Processed Polycrystalline NiTi Shape-Memory Alloys

CARL P. FRICK, ALICIA M. ORTEGA, JEFFREY TYBER, KEN GALL, and HANS J. MAIER

The objective of this study is to examine fundamental processing-structure-property relationships in polycrystalline NiTi bars. Three different polycrystalline Ti-50.9 at. pct Ni (Ti-55.7 wt pct Ni) materials were examined: (1) cast, (2) cast then hot rolled, and (3) cast, hot rolled, then cold drawn. The structure of the materials was investigated at various scales ranging from nanometers to micrometers. The cast materials contained random crystallographic textures along the loading axis of the extracted samples. The hot-rolled and cold-drawn materials contained a strong <111> texture parallel to the deformation-processing direction. The high-temperature hot-rolling process facilitated recrystallization and recovery, and curtailed precipitate formation, leaving the hot-rolled and cold-drawn materials in near solutionized states. The cold-drawn material contained a high density of dislocations and martensite. After a mild aging treatment, all three materials contained distributed coherent Ti_3Ni_4 precipitates on the order of 10 nm in size. The cast material was capable of full shape-memory transformation strain recovery up to approximately 5 pct strain at room temperature under both tension and compression. The hot-rolled and cold-drawn materials demonstrated significant tension-compression stress-strain asymmetry owing to their strong crystallographic texture. Under compression, the deformation-processed materials were only capable of 3 pct transformation strain recovery while under tension they were capable of nearly 7 pct transformation strain recovery. Based on the present results, the presence of small coherent Ti_3Ni_4 precipitates is determined to be the driving force for the favorable strain transformation strain recovery properties in all three materials, despite drastically different grain sizes and crystallographic textures. The unique dependence of elastic modulus on stress-state, temperature, and structure is also presented and discussed for the deformation-processed materials. In addition, we demonstrate that the appearance of a Lüders band transformation under tensile loading can be controlled by material structure. Specifically, the presence of significant martensite and dislocations in the cold-drawn materials was shown to mitigate the Lüders band propagation and result in a more gradual transformation.

I. INTRODUCTION

SHAPE-MEMORY alloys such as nickel-titanium (NiTi) possess the capability to recover relatively large strains induced by mechanical deformation, either spontaneously (pseudoelasticity) or due to application of heat (shape memory). Among numerous other applications, NiTi shape-memory alloys have the potential to enhance civil infrastructure as passive and active structural control members.[1,2] For example, NiTi is a proposed material for large restrainer bars in bridges to reduce the susceptibility of collapse during a severe earthquake.[1] Unlike conventional steel restrainer bars, NiTi is able to dissipate a significant amount of seismic energy by repeatedly regaining large strains under a relatively high force level.[1] Although preliminary studies have demonstrated proof of concept for the use of NiTi in civil structures, cost is one primary inhibiting factor in the widespread implementation of NiTi-based elements in civil structures.

A large fraction of the cost of NiTi materials is inherently linked to the difficulty of processing high-strength NiTi intermetallics into net-shaped forms. Currently, most polycrystalline NiTi materials used in civil, aerospace, and medical applications are formed *via* deformation processing. Deformation processes such as rolling and drawing are necessary for generating the appropriate material shape for specific applications, and are sometimes perceived as essential for generating shape-memory or pseudoelastic properties. However, at present, a fundamental and seamless understanding of the links between deformation processing, the material structure at various scales, and transformation strain recovery properties does not exist. Because of this lack of fundamental understanding, standard processing practice for many NiTi materials is far from optimal and is not based on materials science.

It is imperative to relate typical processing methods in NiTi such as hot rolling and subsequent cold drawing to the induced structure as well as to the stress-strain properties. This fundamental scientific knowledge can be used to tailor processing conditions for property optimization. In the present study we will examine in detail the relationship between processing, structure, and properties in polycrystalline NiTi shape-memory alloy bars. We focus on understanding the fundamental physical links between processing, structure, and relevant properties rather than on a parametric study relating different processing parameters to properties.

Prior experimental work has investigated isolated relationships between deformation processing, transformation temperatures, crystallographic texture, and the stress-strain response of NiTi.[3,4] However, previous work has not linked all of those variables in a continuous manner. In addition, previous studies have concentrated on NiTi thin sheets,[3,4]

CARL P. FRICK and ALICIA M. ORTEGA, Ph.D. Students, JEFFREY TYBER, Master's Student, and KEN GALL, Professor, are with the Department of Mechanical Engineering, University of Colorado, Boulder, CO 80309. Contact e-mail: carl.frick@colorado.edu HANS J. MAIER, Professor, is with the Lehrstuhl für Werkstoffkunde (Materials Science), University of Paderborn, 33095 Paderborn, Germany.

Manuscript submitted August 13, 2003.

single crystals,[5] or wire[6,7] rather than large-diameter bars necessary for civil applications. Furthermore, prior studies typically focus on the effect of cold working, rather than hot rolling, which is commonly used in practice. Although previous studies have examined the structure and properties of NiTi formed by powder metallurgy,[8] cast NiTi is the typical precursor to the rolled/drawn forms and may be a viable material form itself. A potential roadblock to the casting of NiTi is compositional control, as a 0.1 wt pct change in Ni shifts transformation temperatures by 10 to 20 K.[9,10]

Numerous studies have examined the relationship between cold working and transformation temperatures in polycrystalline NiTi.[6,7,11–13] In general, it is known that cold working causes an overall decrease in the austenite and martensite transformation temperatures. This decrease in transformation temperatures is due to a suppression of the martensite phase, caused by an increased dislocation density inhibiting interface mobility.[10,12,14] Residual stresses and defects induced by work hardening cause transformation temperatures to decrease prior to aging.[7,10] In addition, previous work has shown that hot rolling NiTi[15] as well as $Ni_{45.5}Ti_{45.5}Nb_9$[16] causes a decrease in transformation temperatures. Similar to cold working, hot rolling increases dislocation density, impedes the martensitic transformation, and thus lowers transformation temperatures.[12,15,17] However, knowledge of the transformation temperatures is not sufficient to predict key aspects of the stress-strain response of NiTi under various stress-states. Specifically, it is important to understand the effect of deformation processing on recoverable transformation strain levels and stress-strain hysteresis under both tension and compression.

In addition to increasing dislocation density, deformation processing alters the crystallographic orientation and shape of the grains in a polycrystalline material. In NiTi, it is known that a cold-worked material usually has a strong <111> texture,[4,18] although the development of this texture from the cast state has not been studied. Several studies have examined the texture for hot-worked B2 intermetallics with varying results.[19,20,21] The texture distribution for B2 intermetallics may depend on the active slip systems during hot rolling coupled with the rolling parameters such as temperature, reduction ratio, and geometry.[19,20,21] Previous work has demonstrated a <110> texture along the rolling direction in hot-rolled NiTi.[22]

It is well known that crystallographic texture has a significant effect on the stress-strain response of NiTi. Polycrystalline NiTi with a high density of grains oriented with a <111> axis parallel to the loading direction ("<111> texture," for short) will generally demonstrate large recoverable transformation strains in tension.[4,23–25] However, textured NiTi is well known to have an asymmetry between tensile and compressive stress-strain response.[18,23–27] Specifically for a <111> preferred texture, compression will have a relatively high transformation stress, a smaller transformation strain, and a steeper transformation stress-strain slope relative to tension.[23,24,25] Tension-compression asymmetry for polycrystalline NiTi is caused by transformation asymmetry at the single crystal level.[23] Since it is known that polycrystalline NiTi with a <111> texture will behave similarly to a single NiTi <111> crystal,[24,25] the transformation for tension is found to be favored over compression.[23,24,25] Thus, a lower applied stress is needed to transform austenite into martensite in tension. It is also important to note that a difference in the Young's modulus between tension and compression has been observed in polycrystalline NiTi materials.[28] Although an asymmetry of the elastic response has been recognized in the literature, the origin of this effect has not been previously explained.

The objective of this study is to examine fundamental processing-structure-property relationships in polycrystalline NiTi bars. Although the work here will focus on large-diameter NiTi bars, the results are expected to have scientific impact on all polycrystalline NiTi materials that are deformation processed. For example, drawn NiTi tubes are currently used as a vascular stent material,[29] and have a texture similar to that of cold-drawn NiTi bars. The present study will specifically examine cast, hot-rolled, and cold-drawn polycrystalline NiTi bars. The structure of the materials after the different deformation processes will be investigated at various scales ranging from nanometers to micrometers. Thermomechanical analysis will be used to investigate the temperature dependence of the elastic modulus in the different NiTi materials. The basic structural information and thermal characteristics will ultimately be linked with isothermal tensile and compressive stress-strain tests. This fundamental understanding of the material can then be used to tailor the structure of NiTi materials for specific properties.

II. MATERIALS AND EXPERIMENTAL METHODS

Three different polycrystalline NiTi materials were examined in this study: (1) cast, (2) cast then hot rolled, and (3) cast, hot rolled, then cold drawn. The cast material will be referred to as "cast," the cast then hot-rolled material will be referred to as "hot rolled," and the cast then hot-rolled then cold-drawn material will be referred to as "cold-drawn." All three materials have a nominal composition of Ti-50.9 at. pct Ni (Ti-55.7 wt pct Ni). The cast material was solidified in a cylindrical permanent mold with a 70.0-mm diameter. A duplicate cast ingot was subjected to a hot-rolling process at a temperature of between 845 °C and 955 °C. The hot-rolled bar was straightened and centerless ground to yield a final diameter of 31.8 mm. A duplicate hot-rolled bar was cold drawn approximately 30 pct, straightened, and centerless ground to a diameter of 26.7 mm. The fully processed materials were obtained from a commercial supplier.

Test specimens were electrodischarged machined from the three different materials for various types of analysis. Flat dog bone tensile specimens with a 25 mm length and a 3 mm × 1 mm gage cross section and rectangular compressive specimen with dimensions of 4 mm × 4 mm × 8 mm were extracted. The loading axis of the specimens was machined in the direction of the deformation processing and the longitudinal axis in the casting. The specimens from the casting were extracted away from the very top of the ingot where porosity was apparent. Before testing, each specimen was ground to remove all surface oxidation produced by machining and heat treatment (discussed subsequently). Tensile and compressive tests were performed at room temperature (25 °C) and elevated temperature (90 °C) on cast, hot-rolled and cold-drawn samples, using a servohydraulic load frame. Each test was conducted in strain control using a miniature extensometer with a 3-mm gage length. Teflon tape was used during the compression tests to minimize friction effects at the ends of the samples.

Specimens from all three materials were given identical heat treatments at 350 °C for 1.5 hours, to induce coherent Ti_3Ni_4 precipitates in the Ni-rich materials.[30,31,32] The NiTi material prior to heat treatment will be referred to as "as-received." These Ti_3Ni_4 coherent precipitates will be the location of martensite nucleation due to strong local stress fields caused by the lattice mismatch between the precipitates and the matrix.[24] The presence of Ti_3Ni_4 precipitates increases the stress needed for dislocation motion and decreases the critical martensite transformation stress,[24,33] which subsequently improves cyclic stability in NiTi.[34] Furthermore, the chosen heat treatment and degree of cold work will generally result in transformation temperatures below room temperature.[30] Based on these factors, pseudoelasticity is often observed at room temperature for this combination of material composition, deformation processing, and heat treatment.

The overall polycrystalline grain morphology was studied by optical microscopy. Grinding and polishing with polymer-bonded diamond particles prepared optical microscopy specimens. The polished samples were then etched using a solution consisting of 20 ml distilled water, 45 ml glycerin, 25 ml HNO_3, and 1 ml HF for a period of 15 min. This etchant preferentially attacks grains depending on their crystallographic orientations, but does not result in favored etching of the grain boundaries. Thus, the etching results in very small changes in surface topography, which were emphasized by using Nomarski differential interference contrast in the optical microscope.

Crystallographic texture measurements were performed with an X-ray diffractometer. Texture data was obtained from {110}, {200}, and {211} planes in the B2 parent phase and is presented here in the form of inverse pole figures, which were generated using popLA software.[35] Transmission electron microscope (TEM) samples were prepared by mechanical grinding and subsequent twin-jet electropolishing of 3-mm disks. The TEM foils with large electron transparent areas were obtained by electropolishing at 35 V and −15 °C in a 5 pct perchloric acid and 95 pct ethanol solution. The TEM samples were studied in an analytical PHILIPS* CM 200 TEM operated at a nominal acceleration voltage of 200 kV. Samples analyzed after cyclic loading were sliced perpendicular to the loading axis of compression samples.

*PHILIPS is a trademark of Philips Electronic Instruments Corp., Mahwah, NJ.

The elastic modulus of the cast, hot-rolled, and cold-drawn materials as a function of temperature was determined using a dynamic mechanical analyzer (DMA). Samples were tested in three-point bending with a span of 15 mm. The samples were cut to a length of 16.7 mm with a 3 mm × 1 mm cross-sectional area. A static stress of 50 MPa and a dynamic stress of ±10 MPa were applied at a frequency of 1 Hz. The DMA temperature cycle was performed as follows: heat to 100 °C, hold at 100 °C for 5 min, cool to −60 °C at 2 °C/min, and hold at −60 °C for 10 min.

III. EXPERIMENTAL RESULTS

Etched microstructures of the three different polycrystalline NiTi materials are shown in Figure 1. As expected, there is a significant difference in the grain size of the cast material (Figure 1(a)), compared to the hot-rolled and cold-drawn materials (Figures 1(b) and (c) respectively). The cast material shows considerable variability in grain size, escalating to millimeters in size. The average transverse grain size, determined by a linear intersection method on low-magnification images, is 74 μm for the hot-rolled material and 60 μm for the cold-drawn material. Based on the average area difference of the grains in the two materials, a cold work of 35 pct is calculated, which is reasonably consistent with the macroscopic measure of 30 pct.

Figure 2 shows inverse pole figures for the three NiTi materials in the B2 parent phase, which indicates that preferred

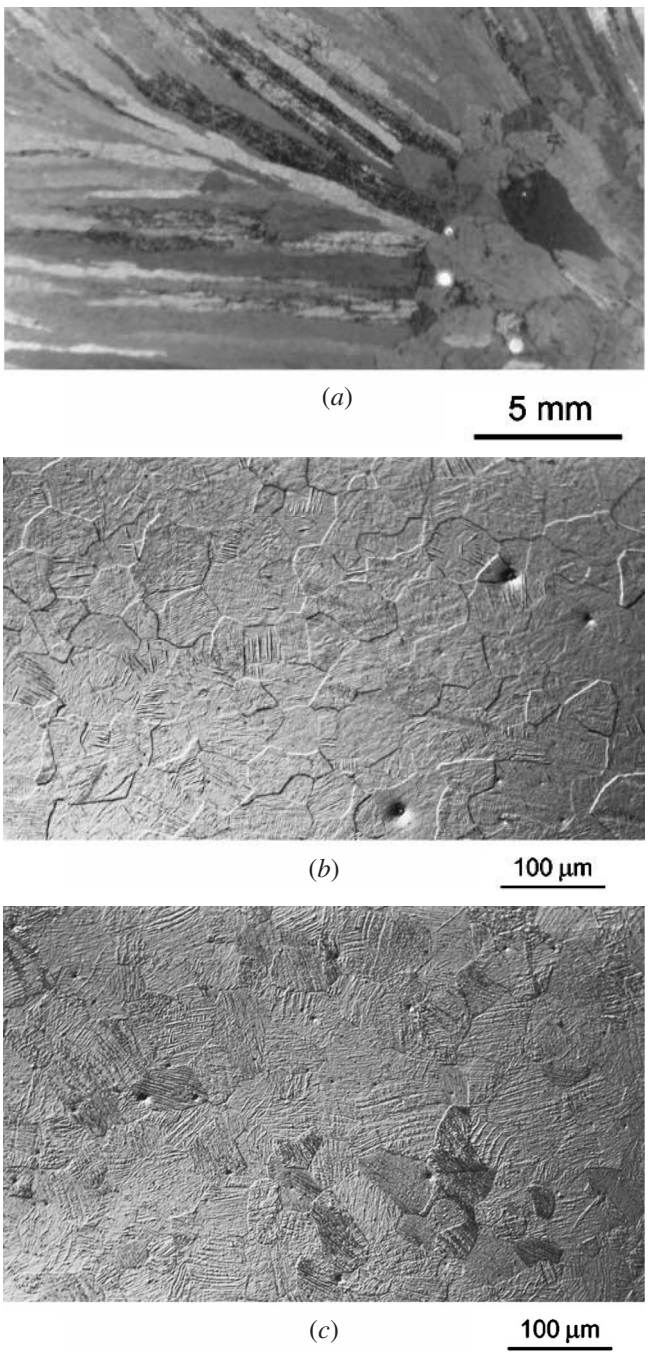

Fig. 1—Microstructure of (*a*) cast polycrystalline NiTi, (*b*) hot-rolled polycrystalline NiTi, and (*c*) cold-drawn polycrystalline NiTi.

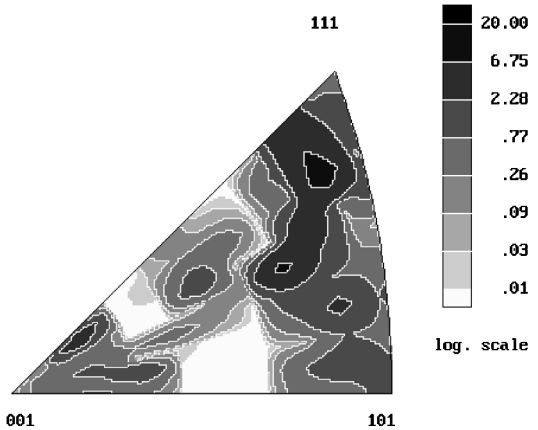

(*a*)

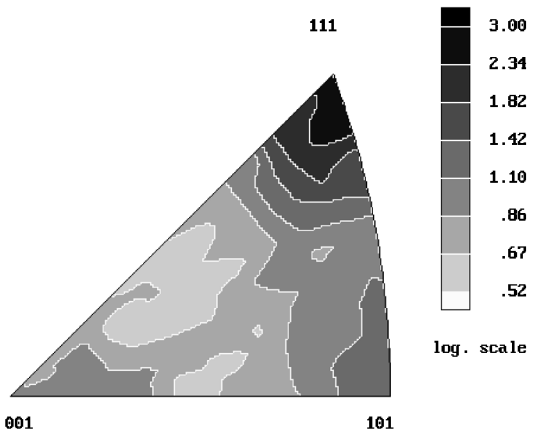

(*b*)

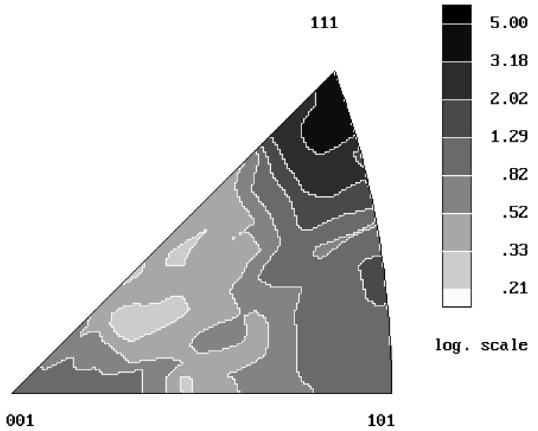

(*c*)

Fig. 2—Inverse pole figures representing texture along the loading direction (equal area projection) for the (*a*) cast, (*b*) hot-rolled, and (*c*) cold-drawn NiTi materials.

grain orientations exist in each material. Figure 2(a) shows some texture peaks in the cast material near the <123>, <117>, and <335> poles, which is a direct result of the spatial differences in solidification conditions, as discussed in more detail later. The inverse pole figure for the hot-rolled material shows a strong fiber texture in the <111> direction (2 to 3 times random) and a moderate texture in the <101> direction (1 to 1.5 times random), as shown in Figure 2(b).

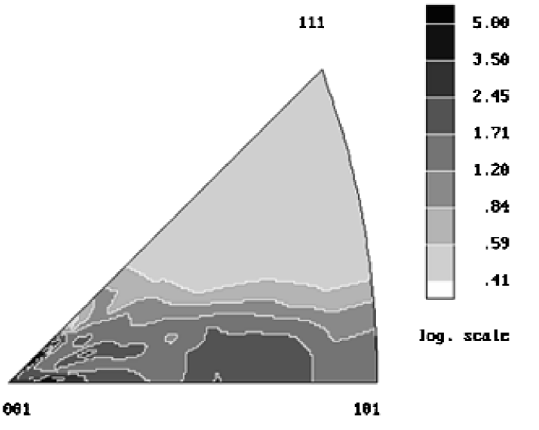

(*a*)

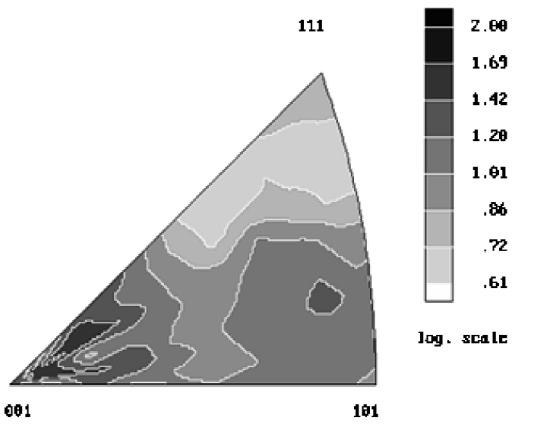

(*b*)

Fig. 3—Inverse pole figures of cast NiTi taken from samples that had been subjected to monotonic (*a*) tension and (*b*) compression testing, showing the materials preferred crystallographic orientation (equal area projection) along the loading direction.

Figure 2(c) shows a strong fiber texture in the <111> direction in the cold-drawn material (3 to 5 times random). Since the microstructure varies spatially in the cast material, as can be seen in Figure 1, an inverse pole figure was obtained from samples that were actually mechanically tested to help provide a direct link between mechanical properties and structure. Figures 3(a) and (b) show the inverse pole figures obtained from tension and compression cast samples, indicating a relatively random distribution of grain orientations in the loading direction.

Figure 4 shows TEM images of the as-received cast, hot-rolled, and cold-drawn materials. Knowledge of the type of precipitate present in NiTi is important, as previous work on single-crystal NiTi[24,25] has shown that precipitates can drastically influence recoverable transformation strain properties as they transition from coherent to incoherent. Figure 4(a) shows the as-received cast material having a microstructure with dislocations present, which is void of larger (>> 10-nm) precipitates. However, the inset in Figure 4(a) which is a higher-magnification dark-field image, demonstrates the presence of localized areas with very small precipitates. Figure 4(b) shows the microstructure of the hot-rolled material prior to heat treatment. The larger grain seen in Figure 4(b), which was imaged using two-beam conditions, shows some mottling on a scale

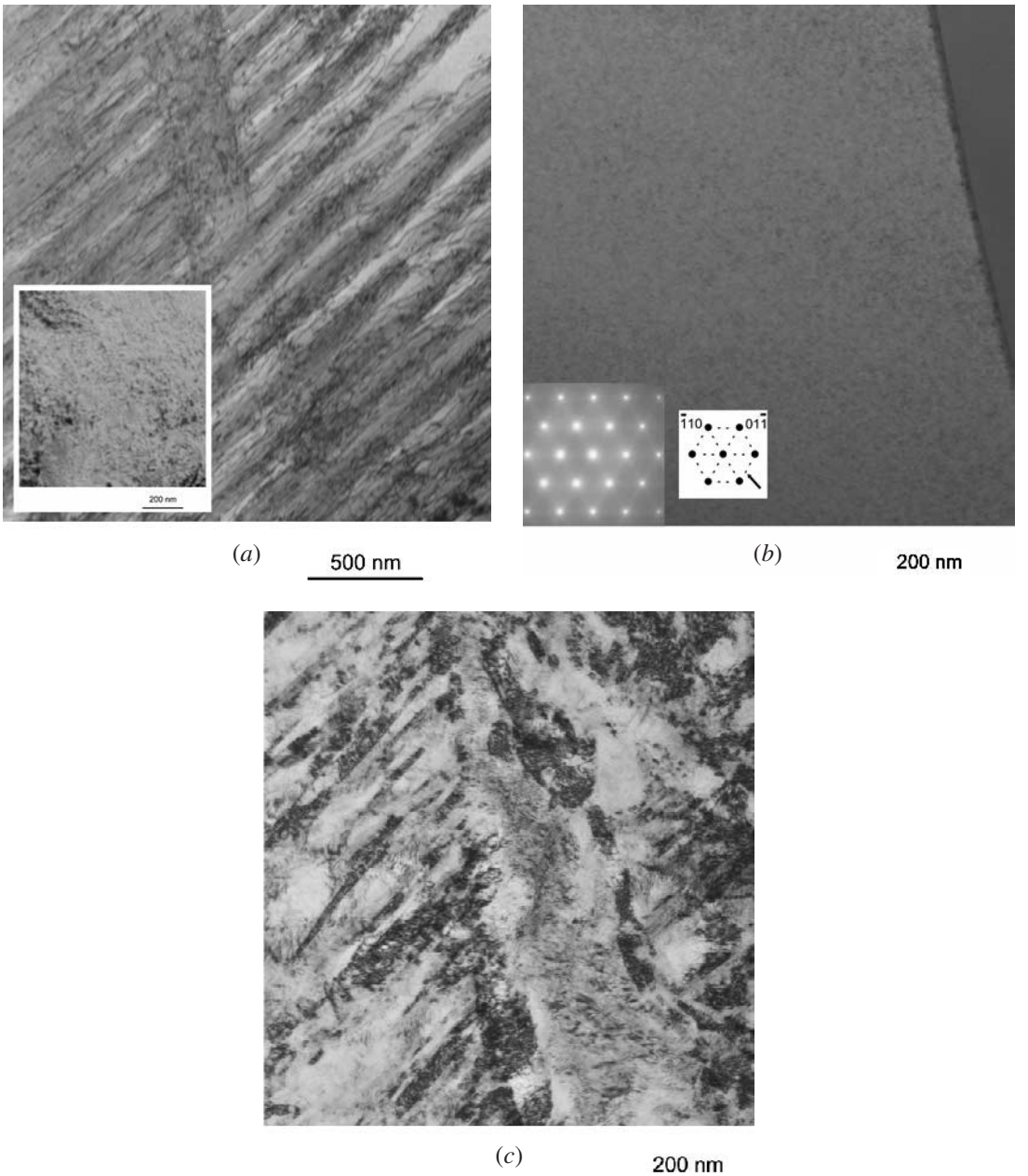

Fig. 4—TEM images of as-received (*a*) cast, (*b*) hot-rolled, and (*c*) cold-drawn materials. Main images were recorded under two-beam bright-field conditions. The inset in (a) is a dark-field image, with contrast reversed to better bring out the few precipitates present. Refer to the main text for details.

less than 10 nm, but precipitates were not clearly resolved in higher-magnification bright-field and dark-field images, respectively. The selected area diffraction pattern shown in the inset was obtained after tilting the specimen to the <111> zone axis. The right inset shows an indexed schematic of the diffraction pattern with diffuse intensity resulting from 1/3 <110> reflections[36] (arrowed). Kompatscher *et al.*[36] studied Ni-rich NiTi alloys and employed small-angle neutron scattering to examine the volume fraction and size of Ti_3Ni_4 precipitates in near solutionized states. In a related study, Somsen[37] obtained diffraction patterns nearly identical to the one inset in Figure 4(b), and the volume fraction and size of Ti_3Ni_4 precipitates was estimated to be below 0.3 vol pct and 1 nm, respectively.[36] The as-received cold-drawn material contained a high density of dislocations and martensite plates, resulting in a heavy strain contrast, as evident in Figure 4(c). The size of precipitates was not confirmed in the as-received cold-drawn material; however, it is reasonable to assume that the precipitates did not grow from their size in Figure 4(b) during the cold drawing.

The TEM images of the cast, hot-rolled, and cold-drawn materials after heat treatment are shown in Figures 5 through 7. Figure 5 shows the presence of small precipitates in the cast material matrix as well as some martensite bands. Figure 6 shows Ti_3Ni_4 precipitates within the NiTi matrix in the heat-treated hot-rolled material. Note that the small precipitates formed after the present heat treatment cause only weak intensities even in overexposed diffraction patterns. For a recent detailed electron microscopy study, the reader is referred to Kompatscher *et al.*[36] and Somsen.[37] For the scope of the present article, it is sufficient to note

that even substantially higher annealing temperatures than those used in the present study will result in coherent precipitates,[31,32] and precipitates will not lose coherency fully before they reach a size of approximately 150 to 300 nm, depending on the degree of cold work.[30]

From the previous TEM observations one expects the microstructure in the heat-treated cold-drawn material to contain precipitates, dislocations, and martensite. The martensite is obvious (Figure 7); the precipitates and dislocations were, however, not individually resolved in high-magnification images due to the strong strain contrast present (Figure 7(b)). In summary, the major microstructural change in all three materials caused by heat treatment is the growth of coherent Ti_3Ni_4 precipitates to an approximate size of 10 nm. The precipitate size is consistent with previous studies on solutionized single-crystal Ti-50.9 at. pct Ni given an identical heat treatment.[34] Previous work has shown that precipitates in NiTi become incoherent with the matrix in the size range of 150 to 300 nm, depending on the degree of cold work.[30,31,32] We note that although the as-received materials contained very small precipitates, the heat treatment noticeably increased the size of these precipitates. This increase in size from the as-received state is critical because the as-received materials showed poor shape-memory properties; the results are not shown here in the interest of space.

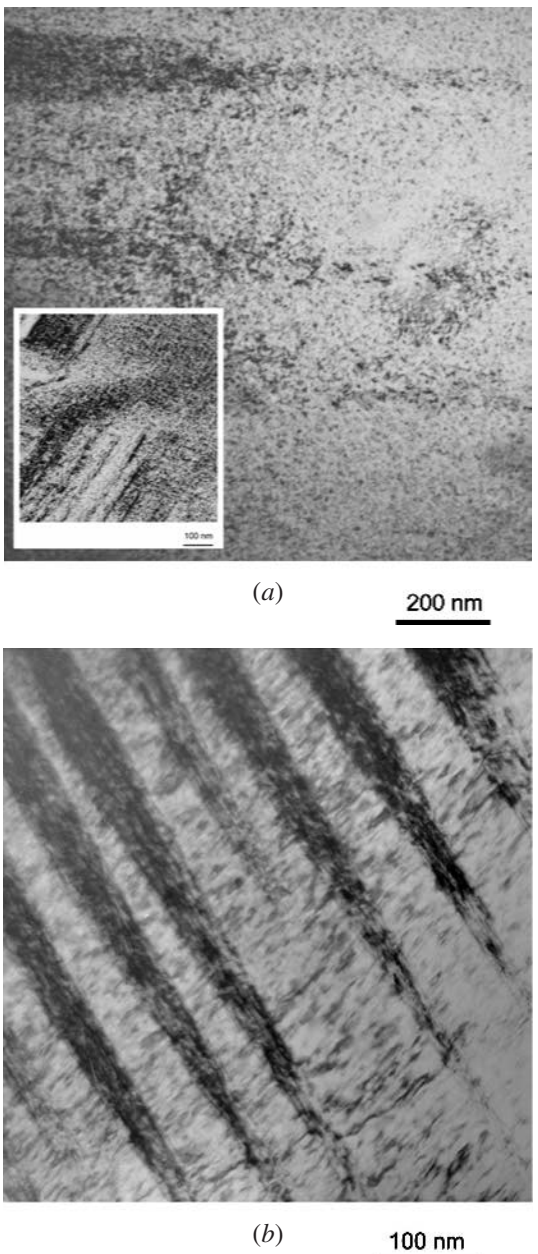

Fig. 5—(*a*) and (*b*) TEM images of aged cast material, showing the presence of small precipitates and bands of martensite. The inset in (a) is a dark-field image recorded at higher magnification that clearly demonstrates the presence of the precipitates. For clarity, contrast has been reversed in the inset.

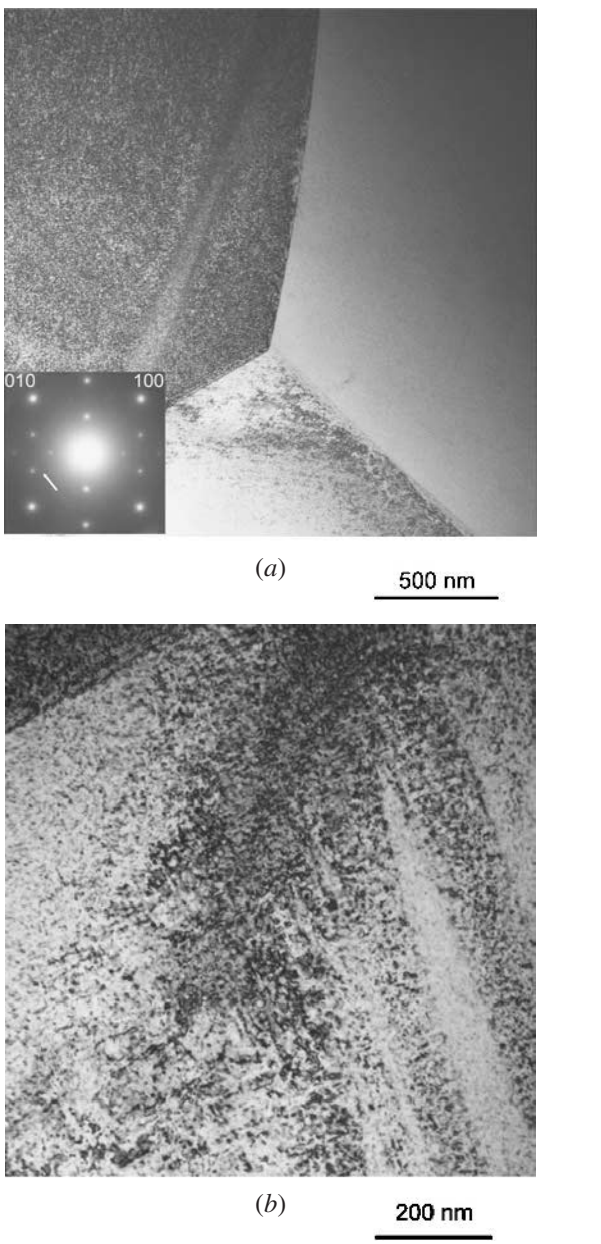

Fig. 6—(*a*) and (*b*) TEM images from the aged hot-rolled material showing typical precipitate density and distribution. Note that the precipitates are distributed homogeneously throughout, but are out of contrast in the grain to the right. The inset is a diffraction pattern obtained after tilting to the [001] zone axis, with 1/3 <110> reflections marked.

The DMA results showing the modulus of all three materials as a function of temperature are presented in Figure 8. All three materials demonstrate a decrease in modulus as they approach their transformation temperatures. The hot-rolled material showed a very sharp drop in modulus (from around 70 to around 45 GPa during a temperature change of only 10 °C to 15 °C), while both the cold-drawn and cast materials showed a more gradual decrease in modulus. It should be noted that the cast material demonstrated the least variation in modulus, varying by only 10.7 GPa across the entire temperature range of −60 °C to 100 °C. In addition, the high-temperature parent phase of the cast material showed a consistently lower elastic modulus. Two exemplar cast specimens were tested and showed nearly identical curves.

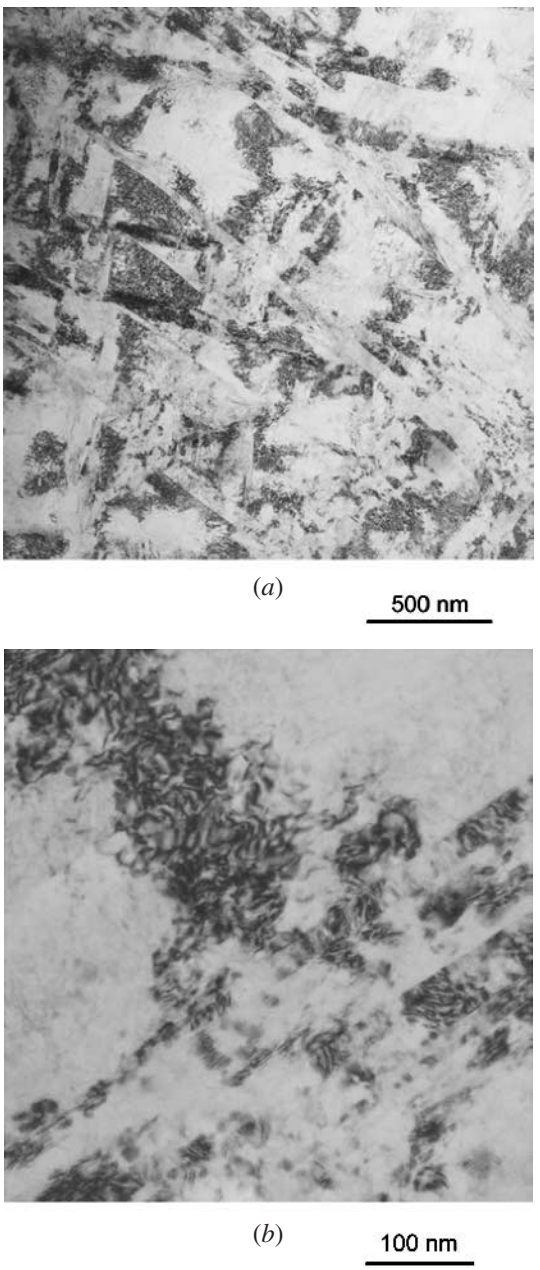

Fig. 7—(*a*) and (*b*) TEM images of the microstructure of the aged cold-drawn NiTi, showing the presence of martensite and large strain contrast due to the combined effect of coherent precipitates and dislocations.

Figure 9 shows the monotonic stress-strain relations for the three NiTi materials under tension and compression. The cast material (Figure 9(a)) demonstrates symmetric shape-memory behavior for the compressive and tensile stress-strain curves with similar transformation stresses and transformation strains up to 5 pct applied strain (Table I). Both the hot-rolled and cold-drawn materials show asymmetric pseudoelastic behavior between their tensile and compressive stress-strain curves, a characteristic behavior of textured polycrystalline NiTi.[23–27] For the deformation-processed materials, the compressive stress-strain response demonstrates higher transformation stresses and smaller transformation strains compared to the tensile response (Table I). It is also interesting to note that in the cast material, the parent-phase loading modulus is similar under tensile and compressive loading. However, in the hot-rolled and cold-drawn materials, a difference in the loading modulus between tension and compression is apparent.

Elevated-temperature (90 °C) stress-strain tests were conducted to obtain the modulus of the three materials at a higher temperature. Not all of these stress-strain curves are presented here in the interest of space, since we were primarily concerned with the elastic response at the higher temperature. The elevated temperature generally resulted in increased loading moduli in all materials tested and a decrease of the tension-compression asymmetry of the elastic modulus (Table I). The compressive response of the cast material at the elevated temperature is shown in Figure 10. In addition to demonstrating a higher loading modulus, the cast material tested at the elevated temperature showed an increase in transformation stress and a switch from shape-memory behavior to pseudoelastic behavior, as expected.

Low-cycle Fatigue tests were conducted on the hot-rolled and cold-drawn material to gain insight into how these two materials behave under cyclic loading, since their monotonic response was similar. Cyclic compression tests were conducted on samples at room temperature (25 °C) to a repeated maximum strain level of 3 pct and a minimum stress level near 5 MPa. As can be seen in Figures 11(a) and (b) both materials saw a decrease in stress hysteresis and an accumulation

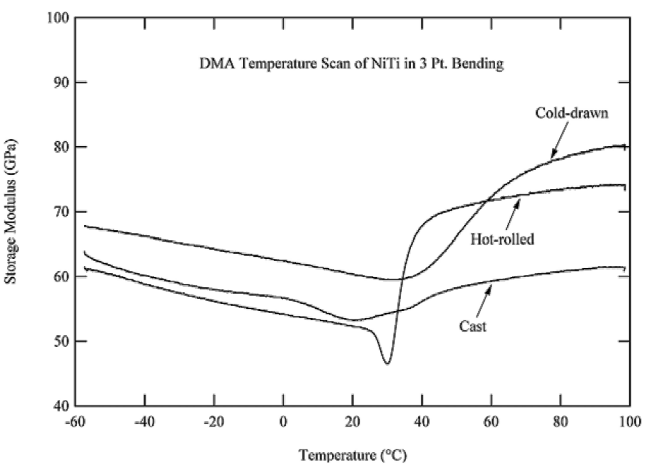

Fig. 8—Storage modulus as a function of temperature for all three polycrystalline NiTi materials. All materials show a decrease in modulus in the range of their transformation temperatures.

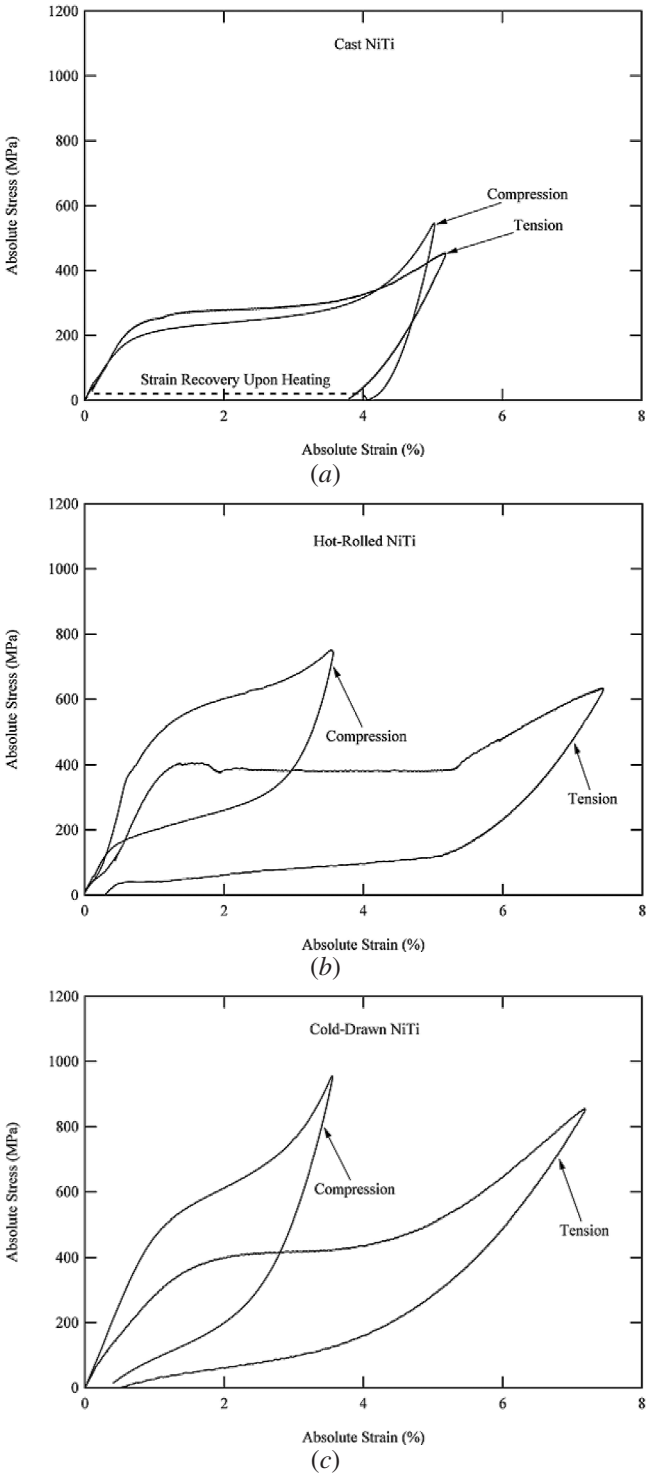

Fig. 9—Room-temperature (25 °C) tensile and compressive stress-strain curves for (*a*) cast, (*b*) hot-rolled, and (*c*) cold-drawn NiTi.

of permanent strains with an increase in cycle number. The TEM images of the hot-rolled and cold-drawn materials, after being cycled 20 times (Figures 12(a) and (b), respectively, show stabilized martensite in both materials.

IV. DISCUSSION

Linking the observed properties and processing to structure *via* the operant deformation mechanisms is the focus of this study. The flowchart in Figure 13 summarizes the effect of the three processing steps on the structure and critical transformation strain recovery properties in NiTi. In this section, we first discuss the relationship between processing and structure followed by a discussion of the relationship between structure and properties in cast and deformation-processed NiTi. Previous studies have examined deformation processing in NiTi; however, it is unclear from these studies which structural variables are playing the strongest role in dictating recoverable transformation strains, since structure was typically only examined at one scale. In the present study we examine and vary the material structure at various scales to ascertain the structural variable(s) most strongly influencing shape-memory properties.

Inspection of the grain structure of the cast NiTi reveals that large grains in the lower right of Figure 1(a) are located at the center of the mold and a columnar structure points radially towards the mold wall. Relatively small grains were present in the portion of the casting in contact with the mold wall. This grain size distribution in the cast material is typical for metals controlled by temperature-gradient-driven solidification in a permanent mold. The samples used for testing and microstructural analysis were extracted closer to the bottom of the mold, where porosity levels were minimal. At the top of the cast piece, in the location of final solidification, the quality of the casting was diminished by noticeable shrinkage porosity. The shrinkage porosity at the top of the casting is an artifact of the solidification and can be minimized by proper casting practice and design. The grain size for both the hot-rolled and cold-drawn materials was relatively uniform and several orders of magnitude smaller than the cast material. The difference in the average transverse grain area between the hot-rolled and cold-drawn materials was approximately 35 pct, consistent with the 30 pct cold working determined *via* overall bar area change. Clearly, the high-temperature hot-rolling process induces dynamic recrystallization of the NiTi from the cast state.

Because the grain size and solidification conditions were dissimilar throughout the cast bar, texture varied spatially. Numerous preferred grain orientations were determined from the texture analysis of the cast bar (Figure 2(a)); however, the spatial locations of these were not examined in detail. An

Table I. Values of Modulus and Recoverable Transformation Strain for NiTi in All Three Materials Obtained from Tensile and Compressive Tests

	E (GPa) 25 °C		*E* (GPa) 90 °C		$\varepsilon_{recoverable}$ (Pct)	
NiTi	Tension	Compression	Tension	Compression	Tension	Compression
Cast	33.6	36.6	62.9	78.1	4.8	4.5
Hot rolled	43.2	86.5	71.1	95	6.8	2.9
Cold drawn	26.1	51.8	85	89	6.4	2.6

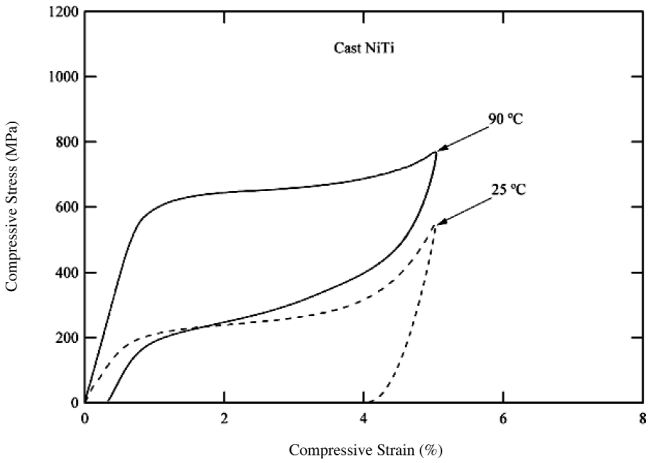

Fig. 10—Elevated temperature (90 °C) compressive response of the cast material compared to the room temperature (25 °C) response.

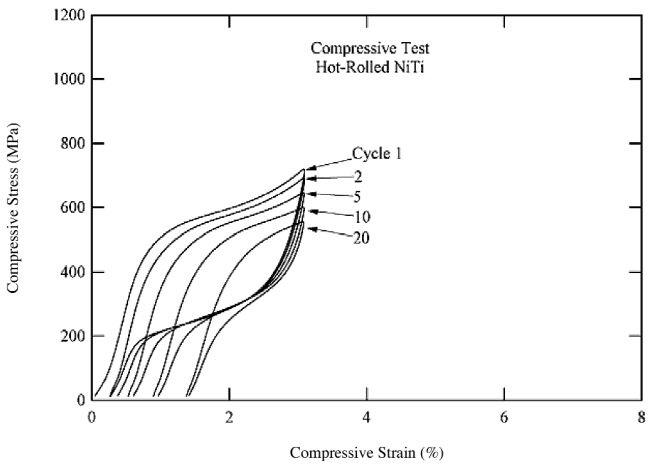

(*a*)

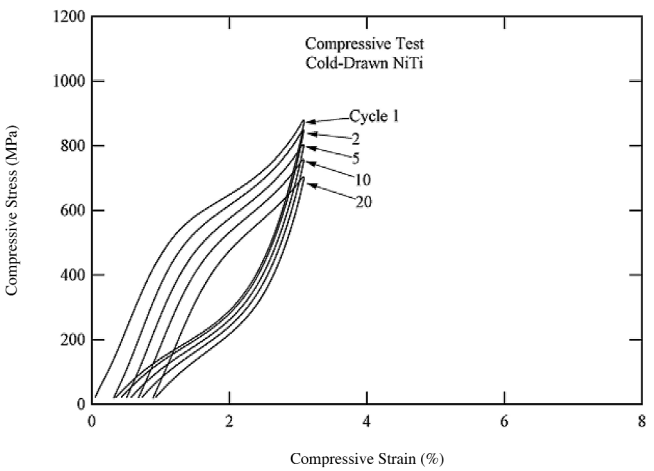

(*b*)

Fig. 11—Cyclic response of the (*a*) hot-rolled and (*b*) cold-drawn materials under compressive loading.

appropriate tool to examine the spatial variation of texture in the cast materials would be electron back scatter diffraction (EBSD). As an alternative approach more appropriate

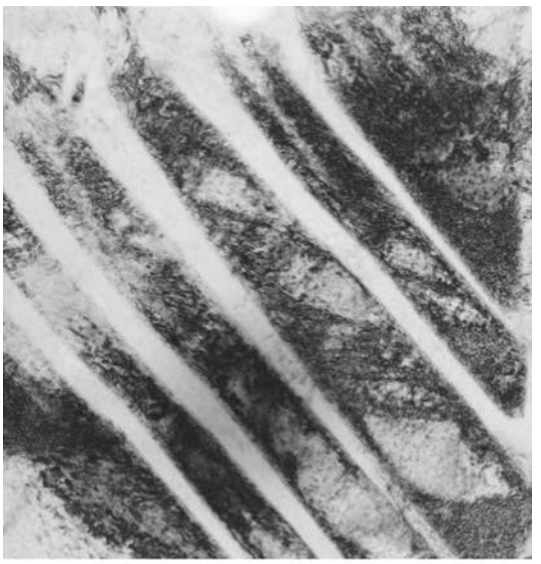

(*a*)

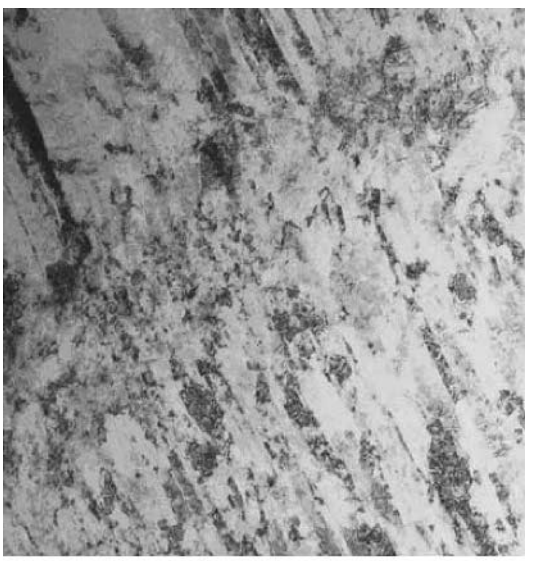

(*b*)

Fig. 12—TEM images of the (*a*) hot-rolled and (*b*) cold-drawn materials after 20 cycles. Both materials show stabilized martensite.

in the current context, we directly measured the texture of the samples used for mechanical testing. The test samples were extracted from the large region of the casting showing radial solidification toward the mold wall (Figure 1(a)). The texture of the samples in the loading direction was basically random, as seen in Figure 3.

The hot-rolled material showed a strong texture, as speculated by Hornbogen[38] in the <111> direction and moderate texture in the <110> direction (Figure 2(b)). Subsequent cold drawing evolves the already strong <111> texture at the expense of the weaker <110> component (Figure 2(c)). Although studies have reported a strong <111> texture in cold-worked NiTi,[4,18] the development of this texture has not been previously linked to the precursory hot-rolling process. In fact, a previous study found that hot-rolled NiTi

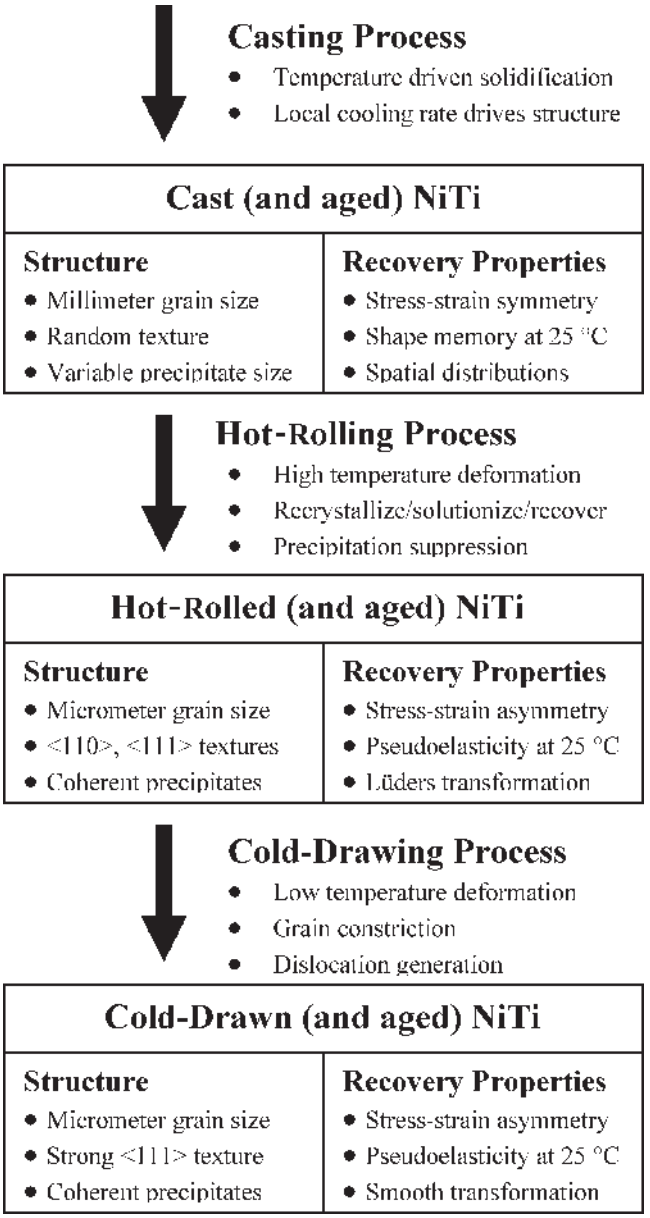

Fig. 13—Schematic of multiscale processing-structure-property relationships in polycrystalline NiTi bars.

developed a <110> crystallographic orientation.[22] However, <111> textures varying in strength have been shown for numerous B2 intermetallics subjected to deformation processing, including FeAl and NiAl alloys.[39] Additionally, the hot rolling of NiAl has been found to induce a strong <111> texture along the rolling axis despite causing dynamic recrystallization,[20] a process that also occurs in hot-rolled NiTi. It is important to note that B2 intermetallics with dissimilar slip systems to NiTi, such as Fe_3Al, do not develop a <111> texture during hot rolling.[21] Consequently, the texture development in NiTi at high temperature ($T > M_d$) is controlled by deformation mechanisms common to some B2 intermetallics not capable of undergoing a thermoelastic martensitic transformation. Potential tailoring of this strong <111> texture component in polycrystalline NiTi must be accomplished at the hot-rolling stage since the cold drawing does not heavily influence the texture development once a strong texture is developed.

The TEM observations of the hot-rolled and cold-drawn materials (Figures 6 and 7) show a Ti_3Ni_4 precipitate size consistent with precipitates formed from solutionized single-crystal Ti-50.9 at. pct Ni materials given the same heat treatment.[34] The high-temperature hot-rolling process occurs between 845 °C and 955 °C, which is above the minimum temperature of 630 °C required to solutionize Ni-rich NiTi, according to the Ni-Ti phase diagram. The minimization of Ti_3Ni_4 precipitation during hot rolling can be accomplished by rapid cooling of the material directly after hot rolling.[30] The cold-drawn material contains precipitates after heat treatment; however, the high density of dislocations induced by deformation processing is not recovered during the mild heat treatment. In fact, aside from the presence of precipitates, the microstructure of the cold-drawn material appears very similar prior to (Figure 4(c)) and after (Figure 7) aging. The minimization of precipitation in NiTi is critical because controlled aging can be used to induce favorable structure and stress-strain properties without solutionizing the hot-rolled and hot-rolled/cold-drawn NiTi materials. Figure 5 also reveals the presence of relatively small precipitates in a cast NiTi sample. However, this TEM image is from a specific region of the casting extracted for mechanical testing, and since precipitate size will change with cooling rate, the precipitate size can vary throughout a complex casting. In all three materials, it is important to recognize that control over the precipitation of Ti_3Ni_4 is absolutely critical. As will be further discussed, the presence of these coherent precipitates ultimately imparts favorable properties to all three materials, dominating the effects of grain size and dislocation density.

We first examine the elastic properties of the three materials *via* DMA analysis. All three materials show a decrease in modulus near their transformation temperatures (Figure 8). The lower elevated temperature modulus of the cast material relative to hot-rolled and cold-drawn materials is consistent with texture measurements; a strong <111> texture possesses the highest elastic modulus relative to other crystallographic orientations. The drop in modulus near the transformation temperatures is caused by the contribution from the martensitic transformation to the elastic modulus measurement. In particular, the highly mobile martensite interfaces[40,41] contribute significantly to the overall strain in the nominal elastic regime, which lowers the apparent modulus of the NiTi. This observation is important since it demonstrates the sensitivity of the NiTi "elastic modulus" near the transformation temperatures to martensite activity.

It is also important to note that the modulus of all three materials below 20 °C is often perceived as the "modulus of the martensite." However, based on the steady increase in the modulus as a function of decreasing the temperature below 20 °C, this measurement is also heavily influenced by the mobility of martensite interfaces. This increase in modulus as a function of temperature is much stronger than the temperature dependence of a typical metal's modulus over this change in temperature. This observation indicates the influence of a temperature-dependent deformation mechanism, such as martensite interface motion, in the elastic measurement. The modulus of the martensite is approaching an actual (higher) value than the value of 28 through

41 GPa[42] traditionally quoted for NiTi shape-memory alloys. For example, the slope of the "elastic" loading region in Figure 9(a) does not represent the actual elastic modulus of the martensite, as this measurement contains significant amounts of strain due to the motion of martensite interfaces. The actual (higher) elastic modulus of the martensite is best represented by the compressive unloading response in Figure 9(c). The unloading modulus under tension in Figure 9(c) is not an accurate measure of the martensite modulus, since it also contains artifacts *via* reverse martensite interface motion.[25]

The elastic modulus at room and elevated temperatures, as determined through uniaxial stress-strain testing (Figures 9 and 10), is presented in Table I. The moduli determined by stress-strain tests are consistent with the "average" moduli determined from the three-point bending thermal analysis in Figure 8. In particular, the difference in the moduli at the low and high temperatures in Table I is consistent with values in Figure 8. It is interesting that, at room temperature, the modulus for the hot-rolled and cold-drawn materials is different in tension *vs* compression. This difference has been previously reported,[28] and been observed here to diminish as the test temperature is increased away from the transformation temperatures. As indicated by the curves in Figure 8, the room-temperature elastic modulus of the materials is heavily influenced by the transformation. Based on the aforementioned evidence, we assert that the asymmetry of the tensile and compressive response of the elastic modulus is caused by strain contributions related to the transformation, such as martensite interface motion, or premartensitic deformation modes, such as the R-phase. For the deformation-processed materials, the martensitic transformation is heavily favored under tensile loading compared to compressive loading, leading to a lower apparent modulus in tension near the transformation temperatures.

The recoverable transformation strains in tension *vs* compression depend strongly on the processing route due to the underlying textures. In Table I and Figure 9(a), it is clear the cast material exhibits a rather symmetric response up to 5 pct strain. On the other hand, deformation-processed materials show a strong asymmetry between recoverable transformation strain levels and the stress-strain response, as has been reported in previous investigations.[24,26,28] The symmetric response of the cast NiTi is an artifact of the random texture in the specimens tested (Figure 3). Although micromechanical modeling has been used to show a symmetric response between tension and compression for polycrystalline NiTi with a random texture,[23] a symmetric response has never been discovered experimentally, due to the deformation-processed materials employed in previous studies. The hot-rolled and cold-drawn materials have a strong <111> texture, which makes the material favorably oriented for the transformation under tension but unfavorably oriented for the transformation in compression. The hot-rolled material contains a mild <110> texture component, which assists the transformation under compression.[23,24]

Although the recoverable transformation strains in the hot-rolled and cold-drawn materials are similar, the transformation proceeds differently in the two materials. In the hot-rolled material deformed under tension, the transformation proceeds through an unstable "Lüders" type (Figure 9(b)), while the transformation is more gradual in the cold-drawn material (Figure 9(c)). Lüders behavior in NiTi is best explained as follows: the stress needed for nucleation of a new phase is higher than the stress needed to propagate that phase.[43] The modulus-temperature curves (Figure 8) also indicate a more gradual transformation in the cold-drawn material compared to the sharp transition observed in the hot-rolled material. The origin of the different transformation progressions in the cold-drawn and hot-rolled materials is rooted in the subgrain microstructure. The dislocations and martensite bands present in the cold-drawn material, consistent with heavy cold working, causes the global martensitic transformation to be less abrupt. The internal stresses caused by the dislocations act to partially inhibit the growth of martensite plates.[10,12,17] On the other hand, the relatively large amount of pre-exisiting martensite needs only to orientate itself favorably with the applied stress. These factors in combination cause a smoother austenite-to-martensite phase transformation. The stress-strain response highlights this phenomenon by having a gradual transformation stress and mild positive stress-strain slope during transformation and reorganization of the martensite. In contrast, the hot-rolled NiTi has virtually no dislocations or pre-existing martensite. As a result, the phase transformation is much more sudden, resulting in Lüders-type behavior. If a Lüders-type transformation is unfavorable, then cold drawing may be a method to mitigate this response from a material standpoint. However, geometrical and loading-rate factors will also control the appearance of such transformation instability, possibly overshadowing this processing effect.

We have also presented preliminary cyclic compression results for the hot-rolled and cold-drawn materials. The purpose of these results is to attempt to differentiate between the two materials, knowing thermomechanically treated nickel rich NiTi typically recovers a large majority of transformation strain under cyclic loading, as opposed to solutionized NiTi.[44] Cyclic stress-strain and TEM results show that both hot-rolled and cold-drawn materials degrade similarly as a function of cycling. Thus, the cold drawing adds little significant benefit when the precipitates are present in the material. Despite cold drawing adding four times the cost of hot rolling, and ten times the cost of casting, based on the purchase costs from a commercial supplier, it was not a major improvement on either the monotonic or cyclic behavior of the stress-strain response. Cold drawing may still be necessary for certain shapes of NiTi, such as wire, but it is not essential for large-diameter NiTi bars to be used in civil engineering applications.

The results presented here have provided new insight into processing-structure-property relationships in NiTi shape-memory alloys. An overarching conclusion of the proposed work is that favorable transformation strain recovery properties can be achieved in cast, hot-rolled, and cold-drawn forms. The favorable shape-memory properties are linked to the presence of small coherent Ti_3Ni_4 precipitates in all three materials. These precipitates favor the transformation by creating preferential martensite nucleation sites and inhibit slip *via* the blocking of dislocation motion.[34] Since the precipitates strongly favor the martensitic transformation, they are the dominant factor for achieving favorable shape-memory properties, far outweighing grain size, for example. Using precipitation treatments to tailor the properties of NiTi is much

more economical then using rather expensive deformation-processing routes. In fact, in thin-film NiTi shape-memory alloys for microelectromechanical systems, deformation processing is not possible, and precipitation treatments are the exclusive means to optimize properties *via* structural changes.

The present work illustrates the importance of selecting the appropriate processing route for NiTi given its functional role in an application. In some applications, cast materials may be sufficient to obtain shape-memory properties at a relatively low cost. In particular, if an application requires large recoverable transformation compressive strains, then untextured cast NiTi materials are the preferred option over heavily deformation-processed materials, which show poor shape memory under compression. Of course, future studies to understand the structure and properties in NiTi castings as a function of solidification conditions are required, since compositional segregation and porosity development during casting could limit or completely circumvent the transformation strain recovery properties of as-cast NiTi materials or products. The hot-rolled and cold-drawn materials are desirable from the standpoint of a more homogeneous microstructure and property distribution. It is unlikely that local regions in these materials will be found that do not transform because of composition problems or casting defects. However, caution should be exercised when prescribing the amount of cold work in NiTi materials. From a structure and property standpoint, hot rolling may be sufficient to obtain homogenized shape transformation strain recovery properties. In some cases, the required geometry may not be attainable exclusively by hot rolling and subsequent cold drawing may be necessary. Regardless, the future cost-effective design of NiTi shape-memory alloy devices should consider the processing required for achieving the necessary structure and transformation strain recovery properties concurrently with geometrical constraints on the material net-shape form.

V. CONCLUSIONS

1. The presence of coherent Ti_3Ni_4 precipitates on the order of 10 nm creates favorable transformation strain recovery properties in cast, hot-rolled, and cold-drawn materials. Grain size was discovered to have a negligible effect on transformation strain recoverability in NiTi containing small coherent precipitates, since varying the grain size by several orders of magnitude resulted in similar transformation strain recovery properties.
2. Crystallographic texture was significantly altered by deformation. The cast material possessed a random texture in the direction of the samples extracted for mechanical testing. The hot-rolled materials contained strong <111> and <110> fiber texture components along the rolling axis. During cold drawing, the <111> texture evolved at the expense of the <110> texture, resulting in a strong <111> fiber texture in the cold-drawn material.
3. The deformation-processed polycrystalline NiTi demonstrated an asymmetry in the tension and compression elastic modulus at testing temperatures near its transformation temperatures. The asymmetry is caused by the favorable contribution of the martensitic deformation mechanisms or premartensitic phenomenon in the materials deformed under tension *vs* compression.
4. Cast NiTi with a random texture distribution showed no asymmetry of recoverable transformation strains between tension and compression up to a strain of 5 pct. This is the first experimental observation of recoverable transformation strain symmetry in NiTi deformed under tension *vs* compression. By contrast, both hot-rolled and cold-drawn materials showed a significant tension-compression asymmetry of the stress-strain response. These observations, for the first time, corroborate theoretical models predicting that NiTi with a random texture will show symmetric transformation strain recovery in tension and compression.
5. The modulus of the NiTi below the martensite finish temperature increases rapidly as temperature is decreased, indicating the suppression of an active deformation mechanism. Near the transformation temperatures, strain contribution due to the martensitic phenomenon lowers the apparent modulus of the martensite as commonly measured through isothermal stress-strain tests and as traditionally quoted in the literature.
6. A Lüders band transformation was observed under tension in the hot-rolled material, but not in the cold-drawn material. This difference is attributed to the microstructure of the cold-drawn material, which contains pre-existing martensite and dislocations induced during room-temperature deformation processing.

ACKNOWLEDGMENTS

The U.S. authors are grateful for the financial support of this work from the Department of Energy through a Presidential Early Career Award for Scientists and Engineers (PECASE). HJM thanks Deutsche Forschungsgemeinschaft for financial support.

REFERENCES

1. R. DesRoches and M. Delemont: *Eng. Struct.*, 2002, vol. 24, pp. 325-32.
2. C.A. Rogers: *J. Intelligent Mater. Systems Struct.*, 1995, vol. 6, pp. 4-12.
3. Y. Liu, Z.L. Xie, J. Van Humbeeck, and L. Delaey: *Acta Mater.*, 1999, vol. 47, pp. 645-60.
4. S. Miyazaki, V.H. No, K. Kitamura, A. Khantachawana, and H. Hosoda: *Int. J. Plasticity*, 2000, vol. 16, pp. 1135-54.
5. H. Sehitoglu, I. Karaman, R. Anderson, X. Zhang, K. Gall, H.J. Maier, and Y. Chumlyakov: *Acta Mater.*, 2000, vol. 48, pp. 3311-26.
6. J.M. Legresy, B. Prandi, and G.M. Raynaud: *J. Phys. IV*, 1991, vol. 1, pp. C4 241-C4 246.
7. D.N. Abujudom, P.E. Thoma, and S. Fariabi: *Mater. Sci. Forum*, 1990, vols. 56–58, pp. 565-70.
8. K. Johansen, H. Voggenreiter, and G. Eggeler: *Mater. Sci. Eng.*, 1999, vols. A273–A275, pp. 410-14.
9. W. Tang, B. Sundman, R. Sandström, and C. Qiu: *Acta Mater.*, 1999, vol. 47, pp. 3457-68.
10. P. Filip and K. Mazanec: *Scripta Metall. Mater.*, 1995, vol. 32, pp. 1375-80.
11. T. Todoroki and H. Tamura: *Trans. Jpn. Inst. Met.*, 1987, vol. 28, pp. 83-94.
12. D. Treppmann and E. Hornbogen: *J. Phys. IV*, 1997, vol. 7, pp. C5 211-C 220.
13. D. Treppmann and E. Hornbogen: *J. Phys. IV*, 1995, vol. 5, pp. C2 211-C 216.
14. P. Filip, J. Rusek, and K. Mazanec: *Z. Metallkd.*, 1991, vol. 82, pp. 488-91.
15. H.C. Lin and S.K. Wu: *Mater. Sci. Eng.*, 1992, vol. A158, pp. 87-91.

16. W. Siegert, K. Neuking, M. Mertmann, and G. Eggeler: *Mater. Sci. Forum*, 2002, vols. 394–395, pp. 361-64.
17. J.K. Allafi, A. Dlouhy, K. Neuking, and G. Eggeler: *J. Phys. IV*, 2001, vol. 11, pp. PR8 529-PR8 534.
18. K. Gall, T. Jesse Lim, D.L. McDowell, H. Sehitoglu, and Y.I. Chumlyakov: *Int. J. Plasticity*, 2000, vol. 16, pp. 1189-1214.
19. I. Lee, A.K. Ghosh, R. Ray, and S. Jha: *Metall. Mater. Trans. A*, 1994, vol. 25A, pp. 2017-26.
20. K.J. Bowman, J. Jenny, and S. Kim: *Mater. Sci. Eng*., 1993, vol. A160, pp. 201-08.
21. D. Raabe and J. Keichel: *J. Mater. Res*., 1996, vol. 11, pp. 1694-1701.
22. W.Q. Yuan and S.Q. Yang: *J. Mater. Sci. Lett*., 2002, vol. 21, pp. 443-45.
23. K. Gall and H. Sehitoglu: *Int. J. Plasticty*, 1999, vol. 15, pp. 69-92.
24. K. Gall, H. Sehitoglu, Y.I. Chumlyakov, and I.V. Kireeva: *Acta Mater*., 1999, vol. 47, pp. 1203-17.
25. K. Gall, H. Sehitoglu, R. Anderson, I. Karaman, Y.I. Chumlyakov, and I.V. Kireeva: *Mater. Sci. Eng*., 2001, vol. A317, pp. 85-92.
26. L. Orgéas and D. Favier: *Acta Mater*., 1998, vol. 46, pp. 5579-91.
27. L. Orgéas and D. Favier: *J. Phys. IV*, 1995, vol. 5, pp. C8 605-C8 610.
28. R. Plietsch and K. Ehrlich: *Acta Mater*., 1997, vol. 45, pp. 2417-24.
29. T. Duerig, A. Pelton, and D. Stöckel: *Mater. Sci. Eng*., 1999, vol. A273–A275, pp. 149-60.
30. D. Treppmann, E. Hornbogen, and D. Wurzel: *J. Phys. IV*, 1995, vol. 5, pp. C8 569-C8 574.
31. P. Filip and K. Mazanec: *Scripta Mater.*, 2001, vol. 45, pp. 701-07.
32. J. Kim, Y. Liu, and S. Miyazaki: *Acta Mater*., 2004, vol. 52, pp. 487-99.
33. S. Miyazaki, Y. Ohmi, K. Otsuka, and Y. Suzuki: *J. Phys. IV*, 1982, vol. 43, pp. C4 255-C4 260.
34. K. Gall and H.J. Maier: *Acta Mater*., 2002, vol. 50, pp. 4643-57.
35. J.S. Kallend, U.F. Kocks, A.D. Rollett, and H.R. Wenk: *Mater. Sci. Eng*., 1991, vol. A132, pp. 1-11.
36. M. Kompatscher, B. Deme, G. Kostorz, C. Somsen, and E.F. Wassermann: *Acta Mater*., 2002, vol. 50, pp. 1581-86.
37. C. Somsen: Ph.D. Thesis, University Duisburg, Shaker Verlag, Aachen, 2002.
38. E. Hornbogen: *Mater. Sci. Eng*., 1999, vols. A273–A275, pp. 630-33.
39. P.S. Khadkikar, G.M. Michal, and K. Vedula: *Metall. Trans. A*, 1990, vol. 21A, pp. 279-88.
40. S. Miyazaki, K. Ostsuka, and C.M. Wayman: *Acta Mater*., 1989, vol. 37, pp. 1873-84.
41. S. Miyazaki, K. Ostsuka, and C.M. Wayman: *Acta Mater*., 1989, vol. 37, pp. 1885-90.
42. J.R. Davis, D. Hodgson, M. Wu, and R. Biermann: *ASM Handbook*, 10th ed., ASM INTERNATIONAL, Materials Park, OH, 1990, vol. 2, p. 899.
43. J. Shaw and S. Kyriakides: *Acta Mater*., 1997, vol. 45, p. 683.
44. A. Heckman and E. Hornbogen: *Mater. Sci. Forum*, 2002, vols. 394–395, pp. 325-28.